




Revealing the $\chi_{\text{eff}}-q$ correlation among Coalescing Binary Black Holes and Evidence for AGN-driven Hierarchical Mergers

YIN-JIE LI * (李银杰) ¹, YUAN-ZHU WANG * (王远瞩) ², SHAO-PENG TANG (唐少鹏) ¹, TONG CHEN (陈彤)³ AND YI-ZHONG FAN (范一中) ^{1,4}

¹Key Laboratory of Dark Matter and Space Astronomy, Purple Mountain Observatory, Chinese Academy of Sciences, Nanjing 210023, People's Republic of China

²Institute for Theoretical Physics and Cosmology, Zhejiang University of Technology, Hangzhou, 310032, People's Republic of China

³School of Physical Science and Technology, Inner Mongolia University, Hohhot 010021, People's Republic of China

⁴School of Astronomy and Space Science, University of Science and Technology of China, Hefei, Anhui 230026, People's Republic of China

ABSTRACT

The origin of the correlation between the effective spins (χ_{eff}) and mass ratios (q) of LIGO-Virgo-KAGRA's binary black holes (BBHs) is still an open question. Motivated by recent identification of two subpopulations of the BBHs, in this work we investigate the potential $\chi_{\text{eff}} - q$ correlation for each subpopulation. Surprisingly, the $\chi_{\text{eff}}-q$ correlation vanishes for the low-mass subpopulation if we introduce a second χ_{eff} distribution for the high-mass subpopulation likely originating from hierarchical mergers. The first subpopulation has a narrow χ_{eff} distribution peaking at ~ 0.05 , whose primary-mass function cuts off at $\sim 45M_{\odot}$, in agreement with first-generation BBHs. The second χ_{eff} distribution is broad and peaks at $\mu_{\chi,2} = 0.35_{-0.22}^{+0.18}$, consistent with the expectation of hierarchical mergers formed in the disks of active galactic nucleus (AGNs). We infer $\mu_{\chi,2} > 0$ at 98.7% credible level, and a symmetric χ_{eff} distribution for the second subpopulation is disfavored by $\mathcal{B} \sim 5$. However, negative values of χ_{eff} are also measured, indicating that the hierarchical mergers may take place within both star clusters and AGN disks. We find a Bayes factor of $\ln \mathcal{B} = 5.2$ for two distinct χ_{eff} distributions relative to single χ_{eff} distribution that conditioned on mass ratios. Therefore we conclude that the $\chi_{\text{eff}}-q$ correlation in the entire population can be explained as the superposition of two subpopulations. Additionally, we suggest to use a flexible mass function to reduce the bias in $\chi_{\text{eff}}-q$ correlation that may be introduced by model mis-specification.

Keywords: Binary Black Holes; Gravitational Waves; Stellar Evolution; Active Galactic Nuclei

1. INTRODUCTION

The coalescing binary black holes (BBHs) will provide clues about their formation and evolutionary processes through the parameters of these systems (Mandel & Farmer 2022). In addition to characterizing the marginalized distributions of these parameters, it is also important to investigate the correlations among them (Heinzel et al. 2024; Callister 2024), including mass versus spin (e.g. Tiwari & Fairhurst 2021; Wang et al. 2022;

Li et al. 2024b,a), mass versus mass ratio (Li et al. 2022), spin versus mass ratio (Callister et al. 2021), redshift versus spin (Biscoveanu et al. 2022), and redshift versus mass versus spin (Tiwari 2022; Guo et al. 2024).

Callister et al. (2021), for the first time, reported the anti-correlation between the effective spins (χ_{eff}) and mass ratios (q) of BBHs with data from GWTC-2 (Abbott et al. 2019, 2021a). This anti-correlation was subsequently confirmed by Abbott et al. (2023a) with data from GWTC-3 (Abbott et al. 2019, 2021a, 2024, 2023b). More detailed analysis (e.g., Adamcewicz & Thrane 2022; Adamcewicz et al. 2023) had shown that the $\chi_{\text{eff}}-q$ anti-correlation is not artificial. However, the

* Contributed equally.

The corresponding author: yzfan@pmo.ac.cn (Y.Z.F)

origin of this anti-correlation is still in debate (Callister et al. 2021; Abbott et al. 2023a).

Many simulations suggested that hierarchical mergers in the disks of active galactic nucleus (AGNs) could explain the observed $\chi_{\text{eff}}-q$ correlation (e.g., McKernan et al. 2022; Santini et al. 2023; Cook et al. 2024). The spin orientations and orbital angular momenta of binary black holes (BBHs) will be modulated by the disks, causing the mergers to favor positive effective spins. Additionally, the migration traps in AGN disks will produce mergers involving multiple generations of black holes (BHs) that have unequal masses and larger (positive) effective spins. Previously, we found that the coalescing BHs can be divided into two subpopulations with significantly different spin-magnitude versus component-mass distributions, which are nicely consistent with first- and higher-generation BHs (Li et al. 2024b). We also found that a fraction of the hierarchical mergers have aligned spin tilts and asymmetric mass ratios, which may give rise to the $\chi_{\text{eff}}-q$ anti-correlation.

However, other simulations suggested that certain formation channels of isolated binaries can produce highly spinning and unequal-mass BBHs, particularly the stable mass transfer formation scenario (Banerjee & Olejak 2024). Because the progenitors of unequal BBH systems in the stable mass transfer formation scenario are more likely to efficiently shrink their orbits during the second Roche-lobe overflow, which makes them easier to enter the tidal spin-up regime and later merge due to GW emission (Olejak et al. 2024). Therefore, it is possible that there may be a correlation between the effective spin and mass ratio in first-generation (or low-spin) BBHs, or among potential isolated evolution channels (Wang et al. 2022; Godfrey et al. 2023; Li et al. 2024a).

Therefore, in this study, we delve into the question of whether the anti-correlation between $\chi_{\text{eff}}-q$ in BBHs originates from a superposition of various formation channels / subpopulations (Li et al. 2024b), if it emerges from the evolutionary processes of a single population with a common formation channel (e.g., Banerjee & Olejak 2024), or alternatively, both effects have contributed to the observed correlation. Additionally, we investigate the χ_{eff} distribution in the high-mass range that corresponds to the hierarchical mergers, in order to find out whether these events originate from the AGN disks, or alternatively from the star clusters which exhibits a symmetric χ_{eff} distribution (Payne et al. 2024; Antonini et al. 2024).

This letter is organized as follows: In Section 2 and Section 3, we introduce the methods and the results. In Section 4, we present the conclusions and engage in discussions.

2. METHODS

We use hierarchical Bayesian inference to measure the hyperparameters of population model; see Appendix A for details. Following Abbott et al. (2023a), we adopted 69 BBH events with false alarm rates (FAR) $< 1\text{yr}^{-1}$ in GWTC-3 for analysis. The posterior samples for each BBH event are obtained from `events-zenodo`, and the ‘C01:Mixed’ samples are adopted.

We first use the same $\chi_{\text{eff}} - q$ distribution model as that used in Callister et al. (2021) to fit data of GWTC-3 for comparison. Specifically, the mean and width of the χ_{eff} distribution change linearly with q (referred to as the Base model); see Appendix B.2 for the detailed formula. The rate evolution model is the MD model (Madau & Dickinson 2014), as defined in the Appendix B.3. To reduce the bias that may be introduced by the mis-modeling of primary-mass distribution, we use the concise non-/semi-parametric formula POWERLAW+SPLINE (PS; Edelman et al. 2022; Abbott et al. 2023a) instead of the popular parametric formula POWERLAW+PEAK (PP; Talbot & Thrane 2018; Abbott et al. 2021b), see Appendix B.1 for the details of mass functions. We find the PP model is disfavored compared to the PS model by $\ln \mathcal{B} = 6$, due to its failure in modeling the additional structures in the primary-mass distribution (Li et al. 2021; Tiwari 2022; Edelman et al. 2023; Abbott et al. 2023a; Callister & Farr 2024). With the PP model, we find an anti-correlation between χ_{eff} and q distribution (i.e., $a < 0$) at 99.2% credible level. However, the credibility decreases to 89.8% with the more flexible PS model, indicating that mis-modeling in the primary-mass distribution may introduce bias in measuring the $\chi_{\text{eff}}-q$ correlation; however, the overall tendency remains unchanged, as shown in Figure 1.

Inspired by the investigation of spin-magnitude versus component-mass distribution (Li et al. 2024b), we introduce another χ_{eff} -distribution to capture the secondary subpopulation of BBHs that is consistent with hierarchical mergers. Two kind of models are applied, one is the Mixture model on primary-mass versus effective-spin distribution,

$$\begin{aligned} \pi_{\text{mix}}(m_1, m_2, \chi_{\text{eff}}|\mathbf{\Lambda}) &= P(m_2|m_1; \mathbf{\Lambda}) \\ &[\pi_1(m_1, \chi_{\text{eff}}|\mathbf{\Lambda})(1 - r_2) + \pi_2(m_1, \chi_{\text{eff}}|\mathbf{\Lambda})r_2], \end{aligned} \quad (1)$$

with

$$\pi_1(m_1, \chi_{\text{eff}}|\mathbf{\Lambda}) = \mathcal{PS}(m_1|\mathbf{\Lambda})P(\chi_{\text{eff}}|q; \mu_{\chi,0}, \sigma_{\chi,0}, a, b) \quad (2)$$

and

$$\begin{aligned} \pi_2(m_1, \chi_{\text{eff}}|\mathbf{\Lambda}) &= \mathcal{PL}(m_1 | -\alpha_2, m_{\text{min},2}, m_{\text{max},2}) \\ &\mathcal{G}_{[-1,1]}(\chi_{\text{eff}}|\mu_{\chi,2}, \sigma_{\chi,2}) \end{aligned} \quad (3)$$

where r_2 is the mixed fraction of the second sub-population, \mathcal{PS} and \mathcal{PL} are the PS and power-law primary-mass function, and $\mathcal{G}_{[-1,1]}$ is the truncated Gaussian distribution. $P(m_2|m_1; \Lambda)$ is the normalized secondary-mass distribution conditioned on m_1 , $P(\chi_{\text{eff}}|q; \mu_{\chi,0}, \sigma_{\chi,0}, a, b)$ is the Base model that encodes the $\chi_{\text{eff}} - q$ correlation (Callister et al. 2021), see Appendix B for the definition.

The other model has a more concise formula, i.e., the two χ_{eff} -distributions are modulated by a transition function of the primary mass (see also Wang et al. 2022; Li et al. 2024b; Guo et al. 2024, for similar constructions), hereafter Transition model,

$$\pi_{\text{tran}}(m_1, m_2, \chi_{\text{eff}}|\Lambda) = \mathcal{PS}(m_1|\Lambda)P(m_2|m_1; \Lambda) P_{\text{tran}}(\chi_{\text{eff}}|q, m_1; \Lambda), \quad (4)$$

with

$$P_{\text{tran}}(\chi_{\text{eff}}|q, m_1; \Lambda) = P(\chi_{\text{eff}}|q; \mu_{\chi,0}, \sigma_{\chi,0}, a, b) \frac{1}{1 + e^{(m_1 - m_t)/\delta_t}} + \mathcal{G}_{[-1,1]}(\chi_{\text{eff}}|\mu_{\chi,2}, \sigma_{\chi,2}) \frac{1}{1 + e^{(m_t - m_1)/\delta_t}}, \quad (5)$$

where m_t and δ_t are the location and rapidness of the transition. For the BBHs with primary mass below / above m_t , the χ_{eff} distribution is dominated by the Base model / second Gaussian distribution.

3. RESULTS

Table 1. Model comparison

Model	$\ln \mathcal{B}$
Base(PS)	0
Base(PS) with $a = 0, b = 0$	0.8
Transition(PS)	3.1
Transition(PS) with $a = 0, b = 0$	5.2
Mixture(PS)	2.1
Mixture(PS) with $a = 0, b = 0$	4
Base(PP)	-5.9
Base(PP) with $a = 0, b = 0$	-6.9
Transition(PP) with $a = 0, b = 0$	-3

Note: All the log Bayes factors are relative to the Base model that encode the $\chi_{\text{eff}}-q$ correlation and accompanied with PS mass function.

In Table 1, we summarize the Bayes factors of the novel models in this work compared to the Base model. The Transition model and Mixture model are more favored than the Base model, with $\ln \mathcal{B} = 3.1$ and $\ln \mathcal{B} =$

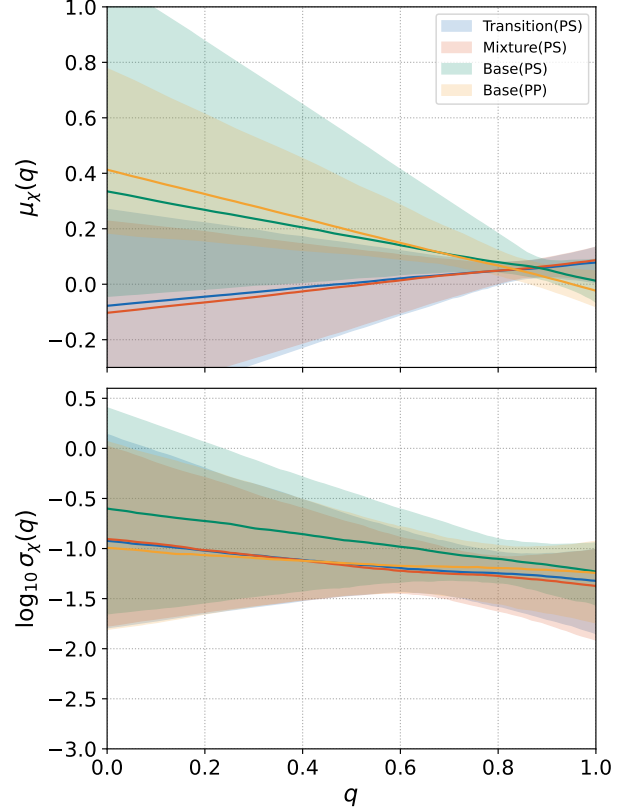


Figure 1. Constraints on the mean $\mu_{\chi}(q)$ and standard deviation $\sigma_{\chi}(q)$ of the χ_{eff} distribution, as a function of BBH mass ratio q . The solid curves are the medians and the colored bands are the 90% credible intervals.

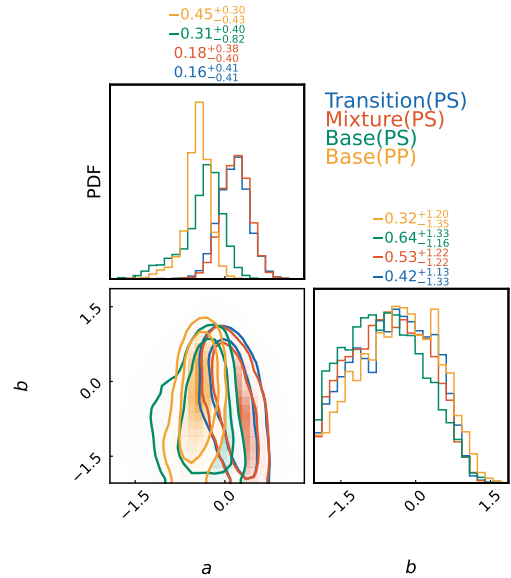


Figure 2. Posteriors of the hyperparameters describing the $\chi_{\text{eff}} - q$ correlation. The contours mark the central 50% and 90% posterior credible regions, the values represent the median and 90% credible intervals.

2.1. Furthermore, the Transition model and Mixture model without the $\chi_{\text{eff}}-q$ correlation (i.e., $a = 0, b = 0$) are even more favored. Figure 2 shows the posteriors of the hyperparameters describing the χ_{eff} and q correlation, the parameters of the Transition model and Mixture model highly consistent with each other. In both models, the slope parameters a and b are consistent with zero, indicating there is no evidence for a $\chi_{\text{eff}}-q$ correlation in the first subpopulation or the low-mass range. In subsequent analysis, we adopt the results inferred with $a = 0, b = 0$, although the posterior distributions of parameters are broadly consistent with the results inferred with variable a and b , see Appendix C.

We find that the second subpopulation shows a significantly different χ_{eff} distribution compared to the first subpopulation, see Figure 3. The divergence point (of the Transition model) in the primary-mass function is $m_t = 49_{-10}^{+13} M_{\odot}$, with a transition scale of $6_{-4}^{+4} M_{\odot}$. As for the Mixture model, the maximum mass of the first subpopulation is $\sim 45 M_{\odot}$, which is consistent with the lower edge of the Pair-instability Supernova BH mass gap (Farmer et al. 2019). The minimum mass of the second subpopulation is $\sim 30 M_{\odot}$. These results are consistent with our previous analysis using spin magnitudes of BBHs (Wang et al. 2022; Li et al. 2024b), see Appendix C for the distributions of other related parameters. The χ_{eff} distributions of both subpopulations are not symmetric with respect to zero, indicating the presence of formation channels other than star clusters.

We find that $\mu_{\chi,2} > 0$ at 98.7% credible level, and a symmetric χ_{eff} distribution with respect to zero for the second population (i.e., $\mu_{\chi,2} = 0$) is disfavored by a Bayes factor of $\ln \mathcal{B} = 1.6$ ($\mathcal{B} \sim 5$), which indicates that the hierarchical mergers cannot be produced (solely) by star clusters. The second χ_{eff} distribution is broad and peaks at $\mu_{\text{eff},2} = 0.34_{-0.22}^{+0.17}$, which is typical for the hierarchical mergers in the AGN disks (Yang et al. 2019). We have also inferred with variable edges ($\chi_{\text{min}}, \chi_{\text{max}}$) truncated on the second χ_{eff} distribution, see Appendix D. Though the case $\chi_{\text{min}} = 0$ cannot be ruled out, the location of the lower edge prefers a negative value. Therefore, it is likely that the star clusters also contribute to the hierarchical mergers.

4. CONCLUSIONS AND DISCUSSION

In this work, we investigate the origins of $\chi_{\text{eff}}-q$ correlation in the BBHs with data of GWTC-3. Different from the previous analysis (Callister et al. 2021; Abbott et al. 2023a), we adopt a more flexible primary-mass function (e.g., PS; Edelman et al. 2022). We find the evidence for the $\chi_{\text{eff}}-q$ anti-correlation inferred with the PS model is weaker than that inferred with the PP model

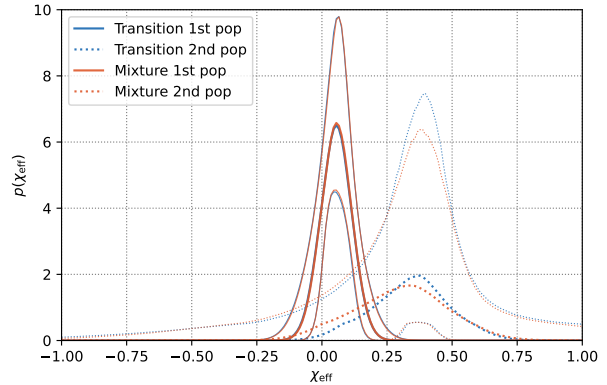


Figure 3. Effective-spin distributions of the two subpopulation inferred by the Transition and Mixture models with $a = 0, b = 0$. The lines represent the mean values and 90% credible intervals

(Talbot & Thrane 2018; Abbott et al. 2021b). This indicates that the parametric formula PP may introduce bias in the $\chi_{\text{eff}}-q$ distribution, since there are additional structures in the primary-mass distribution beyond one power law plus one peak (Abbott et al. 2023a; Tiwari 2022; Edelman et al. 2023; Callister & Farr 2024).

With the dedicated models that introduce a second χ_{eff} distribution for the second (high-spin) subpopulation, the inferred $\chi_{\text{eff}}-q$ correlation vanishes. Therefore, we can conclude that the $\chi_{\text{eff}}-q$ anti-correlation of the entire BBH population mainly results from the superposition of two subpopulations. Additionally, there is no evidence for a $\chi_{\text{eff}}-q$ correlation in each subpopulation identified by the previous work (Li et al. 2024b,a), see Appendix E.

What are the second subpopulation? We point to the hierarchical mergers in gas-rich environments, such as AGN disks (Yang et al. 2019). Our previous works (Wang et al. 2022; Li et al. 2024b) identified a subpopulation of hierarchical mergers in BBHs, providing smoking-gun evidence, specifically a spin-magnitude distribution of approximately 0.7 (Gerosa & Fishbach 2021). Antonini et al. (2024) attributed this subpopulation to hierarchical mergers in star clusters, as they found that the χ_{eff} distribution is consistent with a uniform distribution in the range of approximately (-0.5, 0.5). In this work, we employ a more flexible model and find that the high-spin subpopulation prefers an asymmetric χ_{eff} distribution (with respect to zero) over a symmetric one, with a logarithmic Bayes factor of $\ln \mathcal{B} = 1.6$ (where $\mathcal{B} \sim 5$). we also infer that the peak of the second χ_{eff} distribution $\mu_{\chi,2} > 0$ at 98.7% credible level.

Many simulations (e.g., Yang et al. 2019; Santini et al. 2023; Cook et al. 2024) show that the hierarchical merg-

ers in disk-like environments can produce a χ_{eff} distribution peaking at ~ 0.35 , which is consistent with our results, $\mu_{\chi,2} = 0.35^{+0.17}_{-0.22}(0.30^{+0.19}_{-0.19})$, from the Transition (Mixture) model. However, contribution of formation channels that can produce significantly negative χ_{eff} values, such as hierarchical mergers in star clusters, cannot be ruled out, see Appendix D.

Kick velocities of the merger remnants are also helpful in determining the formation environments of hierarchical mergers (Gerosa & Fishbach 2021; Zevin & Holz 2022; Li & Fan 2024). Several population analyses suggested that the excess of BBHs in $\sim 30 - 40M_{\odot}$ are consistent with the dynamical formation channels (Wang et al. 2022; Li et al. 2024a; Ray et al. 2024), and the ratio of merger rates between hierarchical mergers and first-generation (dynamical) BBHs are consistent with the star cluster origins (Antonini et al. 2023). Therefore, it is possible that the hierarchical mergers detected by LIGO/Virgo/KAGRA originate from both formation environments. However, there are only ~ 11 hierarchical mergers (high-spin events) in GWTC-3 (Li et al. 2024b), making it difficult to determine the mixture fractions of AGN-disk like and star-cluster formation channels. We will address such issue when the GW data are significantly enriched.

Does any single formation channel contributes to $\chi_{\text{eff}} - q$ correlation? (Banerjee & Olejak 2024) We find there is no evidence for a $\chi_{\text{eff}} - q$ correlation in the low-mass sub-populations, which are associated with the first-generation BBHs (Li et al. 2024b). However, this sub-population may not originate from a single formation channel. Both isolated and dynamical formation channels have contributed to first-generation BBHs (Wang et al. 2022; Li et al. 2024b; Godfrey et al. 2023; Li et al. 2024a; Ray et al. 2024). Therefore, we further investigate the $\chi_{\text{eff}} - q$ correlation of BBHs originating from potential formation channels (Wang et al. 2022; Li et al. 2024b; Godfrey et al. 2023; Li et al. 2024a; Ray et al. 2024) and find no evidence for either sub-population. See Appendix E for details. Interestingly, we find a stronger $\chi_{\text{eff}} - q$ correlation in the potential subpopulation associated with the dynamically formed BBHs (i.e., excluding the BBHs from isolated channels as indicated by Li et al. (2024a)). This indicates that the $\chi_{\text{eff}} - q$ correlation originates from dynamical formation channels, and that the AGN-disk formation channels may take a significant contribution (Santini et al. 2023; Cook et al. 2024). The stable mass transfer formation channel is expected to produce BBHs with $\chi_{\text{eff}} - q$

anti-correlation (Olejak et al. 2024; Banerjee & Olejak 2024), while BBHs from the common envelop channel may exhibit an opposite correlation (Bavera et al. 2020, 2021). The $\chi_{\text{eff}} - q$ correlation in the isolated channels may be measured when the detections are enriched and the sup-populations are determined.

The fourth observing run (O4) of the LIGO-Virgo-KAGRA GW detectors is currently underway, and the number of detections is rapidly increasing (see <https://gracedb.ligo.org/latest/>). At the end of O4, more than four times as many events are expected to be observed compared to O3 (Callister 2024). With the enriched data more subpopulations / formation channels of BBHs may be identified (Zevin et al. 2021), and the mixture fractions and the parameter correlations of subpopulations can be better determined (Li et al. 2022, 2024a; Guo et al. 2024; Heinzl et al. 2024; Callister 2024).

- 1 This work is supported by the National Natural Science
- 2 Foundation of China (No. 12233011), the General
- 3 Fund (No. 2024M753495) of the China Postdoctoral Science
- 4 Foundation, and the Priority Research Program of
- 5 the Chinese Academy of Sciences (No. XDB0550400).
- 6 Y-Z Wang is supported by the National Natural Science
- 7 Foundation of China (No. 12203101) and S-P
- 8 Tang is supported by the National Natural Science
- 9 Foundation of China (No. 12303056), the General
- 10 Fund (No. 2023M733736) and the Postdoctoral Fellow-
- 11 ship Program (GZB20230839) of the China Post-
- 12 doctoral Science Foundation. This research has made
- 13 use of data and software obtained from the Gravitational
- 14 Wave Open Science Center ([https://www.gw-](https://www.gwopenscience.org)
- 15 [openscience.org](https://www.gwopenscience.org)), a service of LIGO Laboratory, the
- 16 LIGO Scientific Collaboration and the Virgo Collabora-
- 17 tion. LIGO is funded by the U.S. National Science
- 18 Foundation. Virgo is funded by the French Centre National
- 19 de Recherche Scientifique (CNRS), the Italian Istituto
- 20 Nazionale della Fisica Nucleare (INFN) and the
- 21 Dutch Nikhef, with contributions by Polish and Hun-
- 22 garian institutes.

Software: Bilby (Ashton et al. 2019, version 1.1.4, ascl:1901.011, <https://git.ligo.org/lscsoft/bilby/>), PyMultiNest (Buchner 2016, version 2.11, ascl:1606.005, <https://github.com/JohannesBuchner/PyMultiNest>).

A. HIERARCHICAL BAYESIAN INFERENCE

We perform hierarchical Bayesian inference to infer the hyperparameters Λ describing population models $\pi(\theta|\Lambda)$. Following the framework described in (Mandel et al. 2019; Abbott et al. 2021b, 2023a), given Λ , the likelihood of the GW data $\{d\}$ from N_{det} detections can be expressed as,

$$\mathcal{L}(\{d\}|\Lambda) \propto N^{N_{\text{det}}} e^{-N_{\text{exp}}} \prod_i^{N_{\text{det}}} \int \pi(\theta_i|\Lambda) \mathcal{L}(d_i|\theta_i) d\theta_i, \quad (\text{A1})$$

where N is the total number of mergers in the surveyed time-space volume, which is related to the merger rate density over cosmic history $N = \int R(z|\Lambda) \frac{dV_c}{dz} \frac{T_{\text{obs}}}{1+z} dz$. N_{exp} is the expected number of detections, which is related to the detection probability $P(\text{det}|\theta)$, i.e., $N_{\text{exp}} = N \int P(\text{det}|\theta) \pi(\theta|\Lambda) d\theta$. This term can be calculated using a Monte Carlo integral over the referred injection¹, see Appendix of Abbott et al. (2021b) for details. $\mathcal{L}(d_i|\theta_i)$ is the likelihood of the i -th event, which can be evaluated using the posterior samples (see Abbott et al. 2021b, for detailed illustration).

Following Abbott et al. (2023a); Talbot & Golomb (2023), we define the effective number of samples for the i -th event in the Monte Carlo integral as $N_{\text{eff},i} = \frac{[\sum_j w_{i,j}]^2}{\sum_j w_{i,j}^2}$, where $w_{i,j}$ is the weight of j -th sample in i -th event. We constrain $N_{\text{eff},i} > 10$ to ensure accurate evaluation of likelihood, which is sufficiently high given the sample size of GWTC-3 (Essick & Farr 2022). Additionally, we constrain the effective number of found injections remaining after population reweighting as $N_{\text{eff,sel}} > 4N_{\text{det}}$, to ensure an accurate estimation of N_{exp} (Farr 2019; Abbott et al. 2021b).

B. POPULATION MODELS

B.1. Mass function

The parametric primary-mass function is the popular POWERLAW+PEAK model (Abbott et al. 2021b), which reads,

$$\begin{aligned} \mathcal{PP}(m_1|\Lambda) \propto & \\ & [\mathcal{PL}(m_1 | -\alpha, m_{\text{min}}, m_{\text{max}})(1 - \lambda_{\text{peak}}) + \\ & \mathcal{G}_{[m_{\text{min}}, m_{\text{max}}]}(m_1 | \mu_{\text{m}}, \sigma_{\text{m}}) \lambda_{\text{peak}}] \times \mathcal{S}(m_1 | \delta_{\text{m}}, m_{\text{min}}), \end{aligned} \quad (\text{B2})$$

where $\mathcal{PL}(m_1 | -\alpha, m_{\text{min}}, m_{\text{max}})$ is the Power-law distribution with slope index of $-\alpha$ truncated on $(m_{\text{min}}, m_{\text{max}})$. \mathcal{G} is the Gaussian distribution with mean μ_{m} and width σ_{m} truncated on $(m_{\text{min}}, m_{\text{max}})$, $\mathcal{S}(m_1 | \delta_{\text{m}}, m_{\text{min}})$ is the smooth function with smooth scale of δ_{m} , impacting on the low edge m_{min} .

In order to reduce the bias that may be brought by the mis-specification of parametric formulas, we use a semi-/non-parametric mass function (Edelman et al. 2022) for the main analysis,

$$\begin{aligned} \mathcal{PS}(m_1|\Lambda) \propto & \mathcal{PL}(m_1 | -\alpha, m_{\text{min}}, m_{\text{max}}) \\ & \times \mathcal{S}(m_1 | \delta_{\text{m}}, m_{\text{min}}) e^{f(m|\{x_i\}, \{f_i\})}, \end{aligned} \quad (\text{B3})$$

where $f(m|\{x_i\}, \{f_i\})$ is the cubic-spline perturbation function interpolated between the knots (x_i, f_i) placed in the mass range. Here we adopted 12 knots $\{x_i\}_{i=0}^{12}$ linearly distributed in log space of $(6, 80)M_{\odot}$, and restrict the perturbation to zero at the minimum and maximum knots.

The secondary-mass function is conditioned on the primary mass (Abbott et al. 2021b),

$$P(m_2|m_1; \Lambda) \propto \mathcal{PL}(m_2|\beta, m_{\text{min}}, m_1) \mathcal{S}(m_2|\delta_{\text{m}}, m_{\text{min}}). \quad (\text{B4})$$

B.2. Effective-spin distribution model

We follow Callister et al. (2021) to construct a mass-ratio-dependent model for effective-spin distribution, i.e., the Base model,

$$\begin{aligned} P(\chi_{\text{eff}}|q; \mu_{\chi,0}, \sigma_{\chi,0}, a, b) = & \\ \mathcal{G}_{[-1,1]}(\mu_{\chi}(q; \mu_{\chi,0}, a), \sigma_{\chi}(q; \sigma_{\chi,0}, b)), & \end{aligned} \quad (\text{B5})$$

with

$$\begin{aligned} \mu_{\chi}(q; \mu_{\chi,0}, a) &= \mu_{\chi,0} + a(q - 0.5), \\ \log \sigma_{\chi}(q; \sigma_{\chi,0}, b) &= \log \sigma_{\chi,0} + b(q - 0.5), \end{aligned} \quad (\text{B6})$$

¹ Adopted from <https://zenodo.org/doi/10.5281/zenodo.5636815>.

where $\mathcal{G}_{[-1,1]}$ is the Gaussian truncated on $[-1, 1]$. Note that the linear functions in [Abbott et al. \(2023a\)](#) is slightly different, where the authors let $\mu_\chi(q = 1) = \mu_{\chi,0}$ and $\log \sigma_\chi(q = 1) = \log \sigma_{\chi,0}$.

B.3. Rate evolution model

The merger rate density as a function of redshift reads (MD model [Madau & Dickinson 2014](#)),

$$R(z|\gamma, \kappa, z_p) = R_0 \times \frac{[(1 + z_p)^{(\gamma+\kappa)} + 1](1 + z)^\gamma}{(1 + z)^{(\gamma+\kappa)} + (1 + z_p)^{(\gamma+\kappa)}}, \quad (\text{B7})$$

where R_0 is the local merger rate density. Note the injection campaign only provides mock events with $z < 1.9$, so we normalize the redshift distribution $P(z|\gamma, \kappa, z_p)$ within $(0, 1.9)$, when calculating likelihood.

Table 2. Summary of model parameters.

Parameter	Description	Prior
$m_{\text{min}}[M_\odot]$	The minimum mass	$U(2, 10)$
$m_{\text{max}}[M_\odot]$	The maximum mass	$U(30, 100)$
α	Slope index of the power-law mass function	$U(-8, 8)$
$\delta_m[M_\odot]$	Smooth scale of the mass lower edge	$U(0, 10)$
β_q	Slope index of the mass-ratio distribution	$U(-8, 8)$
Special for PowerLaw+Peak		
λ_{peak}	Fraction in the Gaussian component	$U(0, 1)$
$\mu_m[M_\odot]$	Mean of the Gaussian component	$U(20, 50)$
$\sigma_m[M_\odot]$	Width of the Gaussian component	$U(1, 10)$
Special for PowerLaw+Spline		
$\{f_i\}_{i=2}^{11}$	Interpolation values of perturbation for mass function	$\mathcal{N}(0, 1)$
Effective-spin distribution model		
$\mu_{\chi,0}$	Mean of χ_{eff} distribution given $q = 0.5$	$U(-1, 1)$
$\lg \sigma_{\chi,0}$	Log width of χ_{eff} distribution given $q = 0.5$	$U(-1.5, 0.5)$
a	Correlation between μ_χ and q	$U(-2.5, 2.5)$
b	Correlation between $\log \sigma_\chi$ and q	$U(-2, 2)$
Rate evolution model		
$\lg(R_0[\text{Gpc}^{-3} \text{ yr}^{-1}])$	Local merger rate density	$U(-3, 3)$
z_p	Peak point for the rate evolution function	$U(0, 4)$
γ	Slope of the power-law regime before z_p	$U(-8, 8)$
κ	Slope of the power-law regime after z_p	$U(-8, 8)$
Transition model		
$m_t[M_\odot]$	The transition point in primary-mass function	$U(20, 70)$
$\delta_t[M_\odot]$	Smooth scale of the transition	$U(0, 10)$
$\mu_{\chi,2}$	Mean of χ_{eff} distribution for secondary subpopulation	$U(-1, 1)$
$\lg \sigma_{\chi,2}$	Log width of χ_{eff} distribution secondary subpopulation	$U(-1.5, 0.5)$
Mixture model		
$m_{\text{min},2}[M_\odot]$	Minimum mass of the secondary component	$U(10, 50)$
$m_{\text{max},2}[M_\odot]$	Maximum mass of the secondary component	$U(50, 100)$
α_2	Index of m_1 distribution in the secondary component	$U(-8, 8)$
$\mu_{\chi,2}$	Mean of χ_{eff} distribution for secondary subpopulation	$U(-1, 1)$
$\lg \sigma_{\chi,2}$	Log width of χ_{eff} distribution secondary subpopulation	$U(-1.5, 0.5)$
r_2	fraction of the secondary component	$U(0, 1)$

Note: U and \mathcal{N} are for Uniform and Normal distribution.

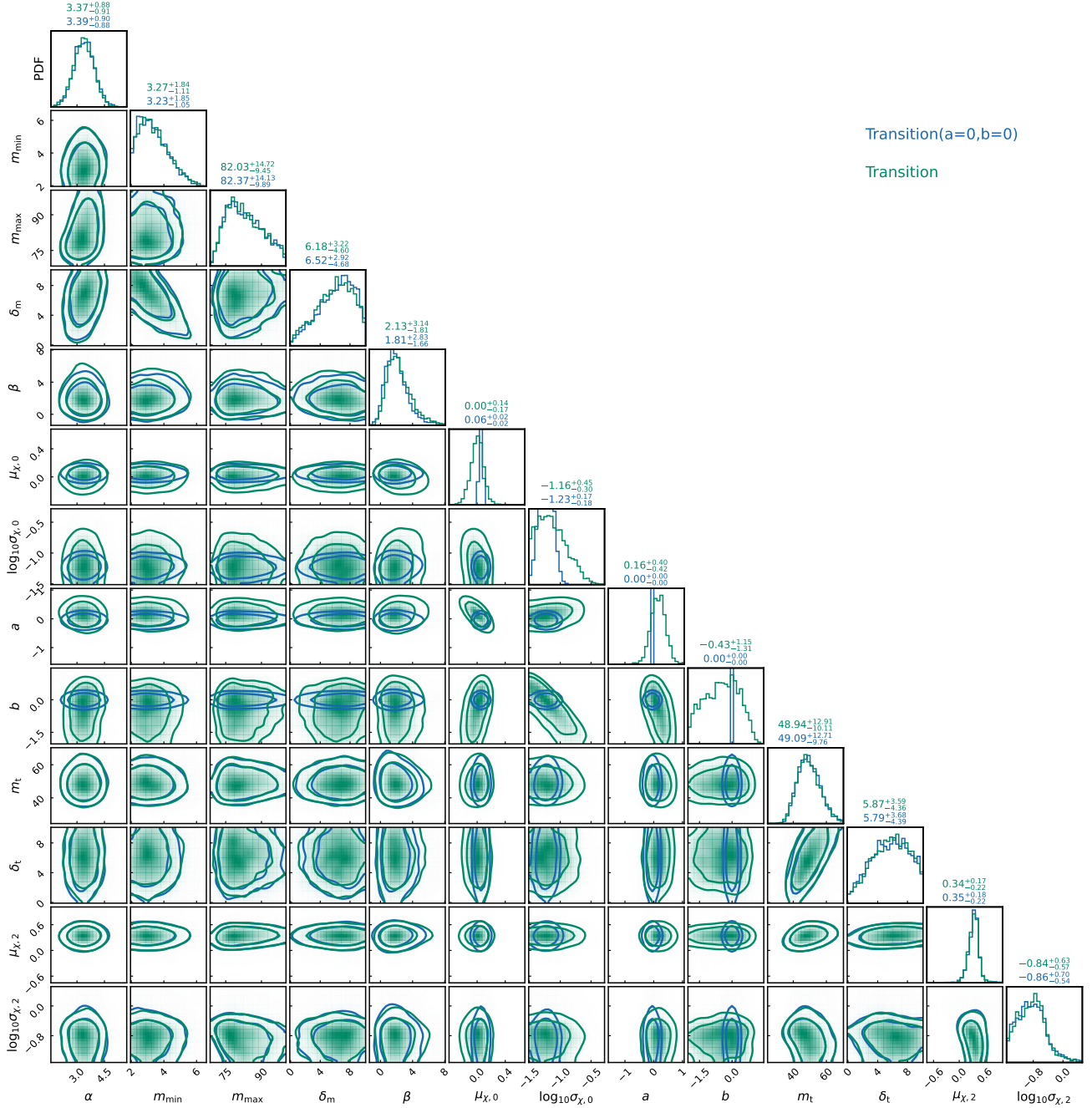


Figure 4. Posteriors of the special hyperparameters for the Transition model. The contours mark the central 50% and 90% posterior credible regions, the values represent the median and 90% credible intervals.

C. ADDITIONAL RESULTS

Figure 4 and Figure 5 present the full hyperparameters (except for the interpolation knots) of the Transition model, and Mixture model respectively. We find that whether we fix $a = 0, b = 0$ or not does not affect the transition / classification of the two subpopulations. These results are consistent with the analysis using spin-magnitude distributions in our previous work (Li et al. 2024b). We observe that the results of the two models are well consistent with each other. The first χ_{eff} distribution narrowly peaks at ~ 0.05 , while the second χ_{eff} distribution peaks at ~ 0.35 , favoring a contribution from hierarchical mergers in AGN disks (Yang et al. 2019).

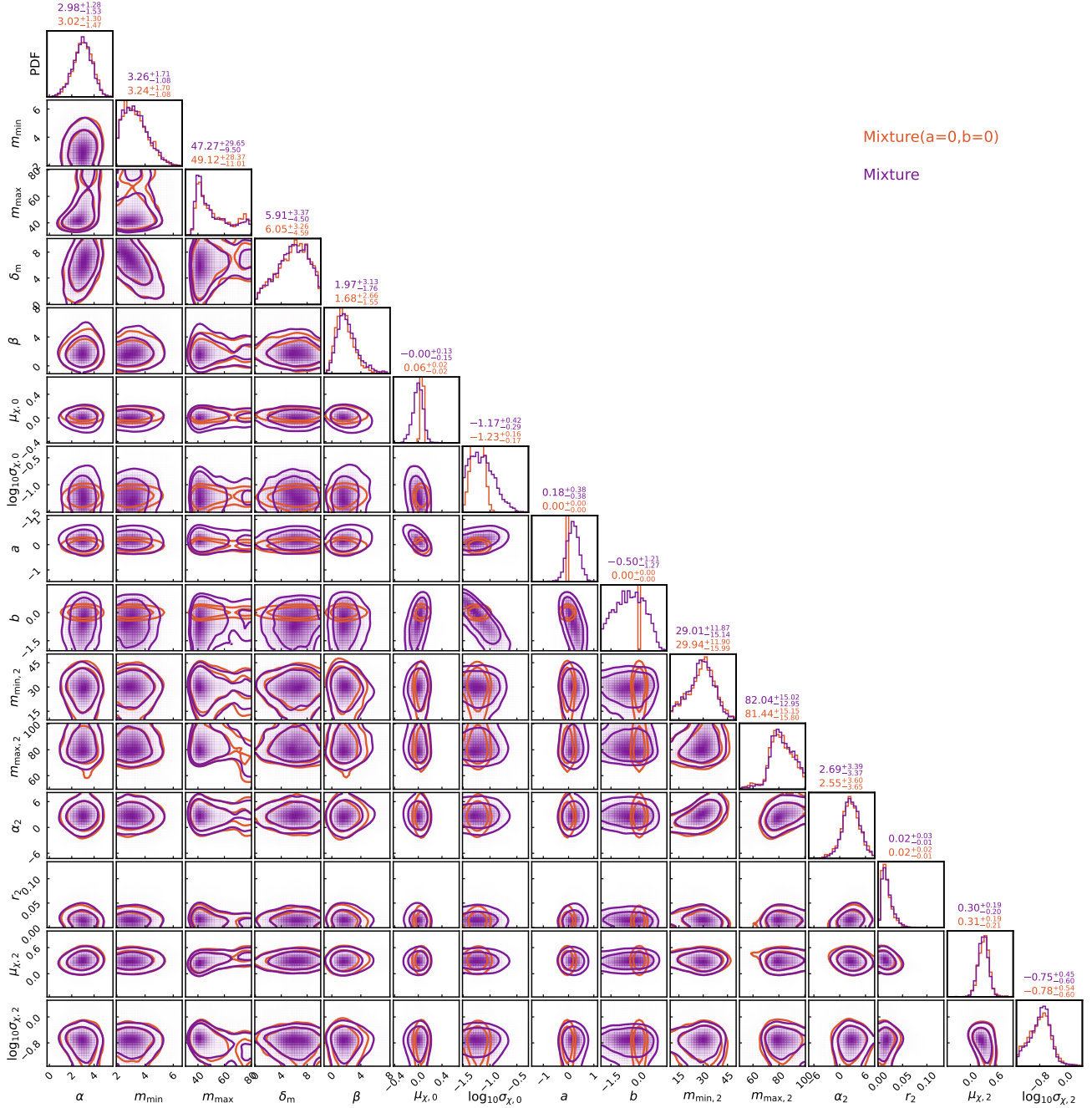


Figure 5. Posteriors of the special hyperparameters for the Mixture model. The contours mark the central 50% and 90% posterior credible regions, the values represent the median and 90% credible intervals.

D. IS THE SECOND χ_{EFF} DISTRIBUTION SYMMETRIC?

The symmetry of χ_{eff} distribution is critical for determining the formation environments of hierarchical mergers. Hierarchical mergers in star clusters always exhibit a symmetric χ_{eff} distribution (Payne et al. 2024; Fishbach et al. 2022). While AGN-driven hierarchical mergers tend to favor positive χ_{eff} due to gas torques (McKernan et al. 2018). In this section, we infer with variable lower edge and upper edge ($\chi_{\min,2}$, $\chi_{\max,2}$) for the second χ_{eff} distribution. We infer that $\chi_{\max,2} > 0.4$ at 97% credible level. Although, we cannot rule out the case of $\chi_{\min,2} = 0$, it is more likely that $\chi_{\min,2}$ takes on a negative value, as shown in Figure 6.

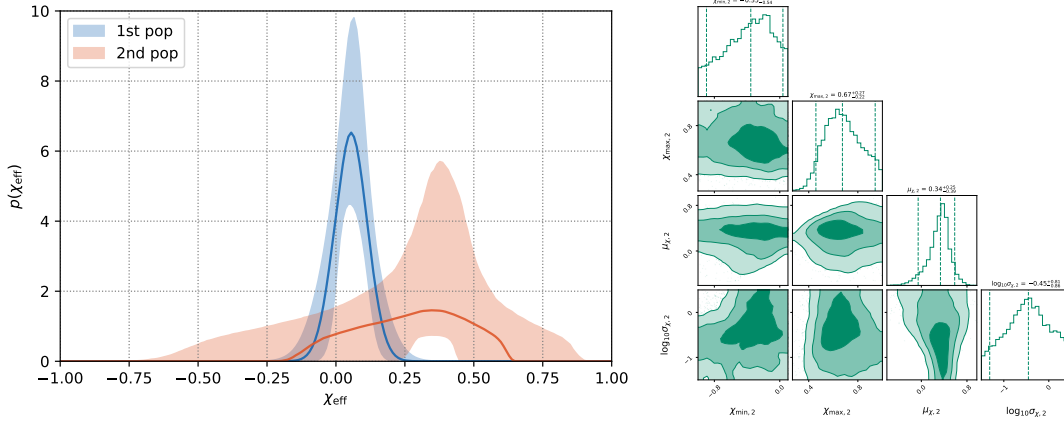


Figure 6. χ_{eff} distributions inferred using Transition with variable edges $\chi_{\text{min},2}$ and $\chi_{\text{max},2}$ truncated on the second χ_{eff} distribution.

E. ARE THERE $\chi_{\text{EFF}} - Q$ CORRELATION IN SUBPOPULATIONS?

As presented in Section 3, we find no evidence for $\chi_{\text{eff}} - q$ correlation in the low-spin (or first-generation) subpopulation. However, the first-generation subpopulation is most likely a mix of BBHs originating from both isolated and dynamical channels (Wang et al. 2022; Li et al. 2024a; Ray et al. 2024). Therefore, it is possible that the $\chi_{\text{eff}} - q$ correlation occurs in a single, specific channel, such as the isolated evolution channel (Banerjee & Olejak 2024).

We first artificially divide the entire population into three subpopulations according to our previous works (see Supplemental Table IV of Li et al. 2024b) and (Table 5 of Li et al. 2024a). The first is the low-spin & nearly-aligned subpopulation, that is related to the isolated evolution channels, see Table 4. The second is the high-spin subpopulation, related to hierarchical mergers, which are also identified within this work. The third is the low-spin & isotropic subpopulation that is associated with the first-generation BBHs formed in star clusters. The reason why we do not jointly fit the three subpopulation in this work is that, it is difficult to distinguish the first and third subpopulations using the χ_{eff} distribution, since the effective spins in both subpopulations are close to zero as shown in Figure 3.

We then fit the three sets of samples with the Base (PS) model, respectively. Figure 7 shows the posterior distributions of the parameters describing the χ_{eff} and q distribution in each potential subpopulation. We find there is no evidence of correlation in either subpopulation, see also Table 3.

Interestingly, if we fit the combination of the second and third sub-set samples, which is potentially associated with the dynamical assembly (Li et al. 2024a), then we find strong evidence for the $\chi_{\text{eff}} - q$ correlation with $\ln \mathcal{B} = 2.6$, see also Figure 7 (Right). This result is consistent with the predictions of mergers in AGN disks (Cook et al. 2024). We find that a significant fraction of BBHs in the 2nd pop have large (positive) χ_{eff} values, while the BBHs in the 3rd pop are located at $\chi_{\text{eff}} \sim 0, q \sim 1$. Therefore, the $\chi_{\text{eff}} - q$ anti-correlation likely arises from the superposition of these two types of subpopulations.

Table 3. Model comparison

Data Sets	$\ln \mathcal{B}_{\text{w./o. corr.}}^{\text{with corr.}}$
Whole	-0.8
Low-Spin Aligned (Field; 1st pop)	-1.2
High-Spin (2G; 2nd pop)	-0.1
Low-Spin Isotropic (Dynamical 1G; 3rd pop)	-1.0
Low-Spin (1G; 1st+3rd pop)	-2.1
Low-Spin Isotropic + High-Spin (Dynamical; 2nd+3rd pop)	2.6

Note: Bayes factor for each potential subpopulation with versus without a $\chi_{\text{eff}} - q$ correlation.

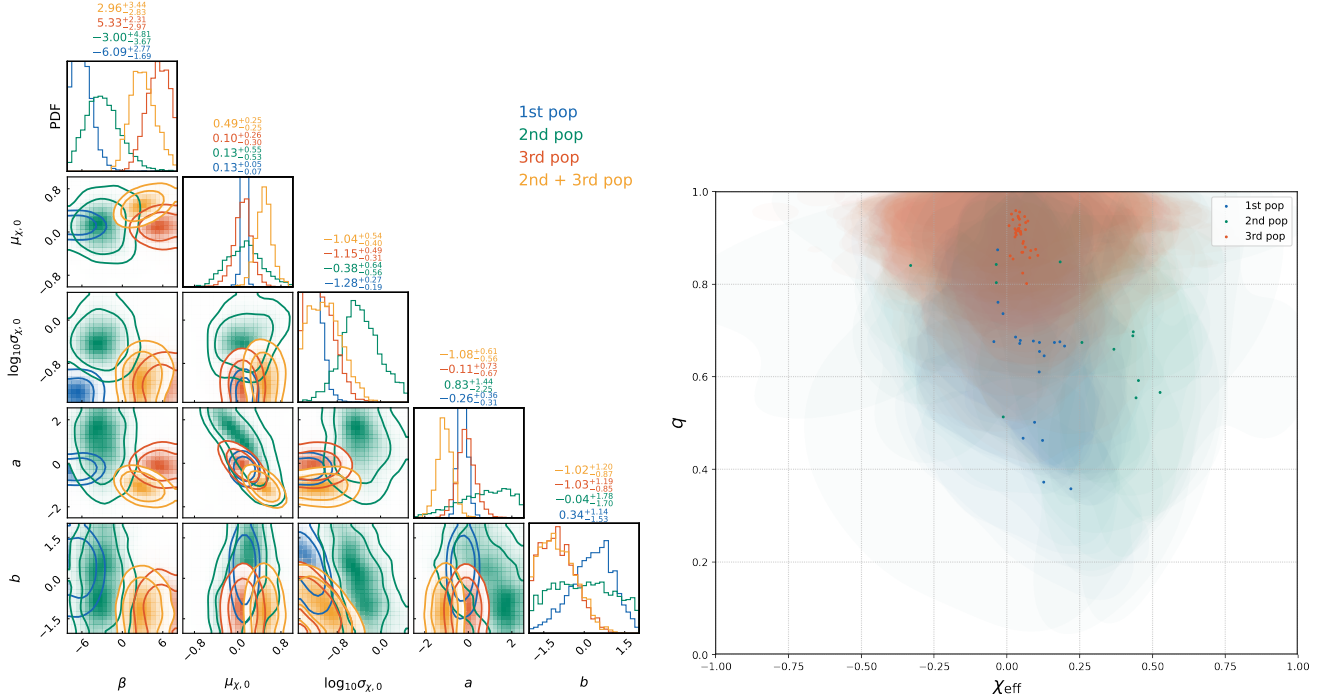


Figure 7. Left: posterior distribution of parameters describing the $\chi_{\text{eff}}-q$ distribution in each subpopulation. Right: posterior $\chi_{\text{eff}}-q$ distribution of individual event reweighed to the population-informed prior. The shaded areas mark the 90% credible regions and the points stand for the mean values.

Table 4. Events of each potential subpopulation

Low-Spin Aligned (Field; 1st pop)					
GW151012.095443	GW151226.033853	GW170608.020116	GW190412.053044	GW190512.180714	GW190707.093326
GW190708.232457	GW190720.000836	GW190728.064510	GW190828.065509	GW190924.021846	GW190930.133541
GW190725.174728	GW191105.143521	GW191129.134029	GW191204.171526	GW191216.213338	GW200202.154313
GW200316.215756	GW191103.012549				
High-Spin (2G; 2nd pop)					
GW170729.185629	GW190517.055101	GW190519.153544	GW190521.030229	GW190602.175927	GW190620.030421
GW190701.203306	GW190706.222641	GW190929.012149	GW190805.211137	GW191109.010717	
Low-Spin Isotropic (Dynamical 1G; 3rd pop)					
GW150914.095045	GW170104.101158	GW170809.082821	GW170814.103043	GW170818.022509	GW170823.131358
GW190408.181802	GW190413.134308	GW190421.213856	GW190503.185404	GW190513.205428	GW190521.074359
GW190527.092055	GW190630.185205	GW190727.060333	GW190803.022701	GW190828.063405	GW190910.112807
GW190915.235702	GW190925.232845	GW190413.052954	GW190719.215514	GW190731.140936	GW191127.050227
GW191215.223052	GW191222.033537	GW191230.180458	GW200112.155838	GW200128.022011	GW200129.065458
GW200208.130117	GW200209.085452	GW200219.094415	GW200224.222234	GW200225.060421	GW200302.015811
GW200311.115853	GW200216.220804				

Note: The 2nd sub-set of GW events are figured out according to [Li et al. \(2024b\)](#), each event has probability > 0.5 to containing at least one high-spin BH. The 3rd sub-set are figured out according to [Li et al. \(2024a\)](#), each event has probability > 0.5 belonging to isotropic-spin sub-population.

REFERENCES

- Abbott, B. P., Abbott, R., Abbott, T. D., et al. 2019, *Physical Review X*, 9, 031040, doi: [10.1103/PhysRevX.9.031040](https://doi.org/10.1103/PhysRevX.9.031040)
- Abbott, R., Abbott, T. D., Abraham, S., et al. 2021a, *Physical Review X*, 11, 021053, doi: [10.1103/PhysRevX.11.021053](https://doi.org/10.1103/PhysRevX.11.021053)
- . 2021b, *ApJL*, 913, L7, doi: [10.3847/2041-8213/abe949](https://doi.org/10.3847/2041-8213/abe949)
- Abbott, R., Abbott, T. D., Acernese, F., et al. 2023a, *Physical Review X*, 13, 011048, doi: [10.1103/PhysRevX.13.011048](https://doi.org/10.1103/PhysRevX.13.011048)
- . 2023b, *Physical Review X*, 13, 041039, doi: [10.1103/PhysRevX.13.041039](https://doi.org/10.1103/PhysRevX.13.041039)
- . 2024, *PhRvD*, 109, 022001, doi: [10.1103/PhysRevD.109.022001](https://doi.org/10.1103/PhysRevD.109.022001)
- Adamcewicz, C., Lasky, P. D., & Thrane, E. 2023, *ApJ*, 958, 13, doi: [10.3847/1538-4357/acf763](https://doi.org/10.3847/1538-4357/acf763)
- Adamcewicz, C., & Thrane, E. 2022, *MNRAS*, 517, 3928, doi: [10.1093/mnras/stac2961](https://doi.org/10.1093/mnras/stac2961)
- Antonini, F., Gieles, M., Dosopoulou, F., & Chattopadhyay, D. 2023, *MNRAS*, 522, 466, doi: [10.1093/mnras/stad972](https://doi.org/10.1093/mnras/stad972)
- Antonini, F., Romero-Shaw, I. M., & Callister, T. 2024, arXiv e-prints, arXiv:2406.19044, doi: [10.48550/arXiv.2406.19044](https://doi.org/10.48550/arXiv.2406.19044)
- Ashton, G., Hübner, M., Lasky, P. D., et al. 2019, *Bilby: Bayesian inference library*, Astrophysics Source Code Library, record ascl:1901.011. <http://ascl.net/1901.011>
- Banerjee, S., & Olejak, A. 2024, arXiv e-prints, arXiv:2411.15112, doi: [10.48550/arXiv.2411.15112](https://doi.org/10.48550/arXiv.2411.15112)
- Bavera, S. S., Fragos, T., Qin, Y., et al. 2020, *A&A*, 635, A97, doi: [10.1051/0004-6361/201936204](https://doi.org/10.1051/0004-6361/201936204)
- Bavera, S. S., Fragos, T., Zevin, M., et al. 2021, *A&A*, 647, A153, doi: [10.1051/0004-6361/202039804](https://doi.org/10.1051/0004-6361/202039804)
- Biscoveanu, S., Callister, T. A., Haster, C.-J., et al. 2022, *ApJL*, 932, L19, doi: [10.3847/2041-8213/ac71a8](https://doi.org/10.3847/2041-8213/ac71a8)
- Buchner, J. 2016, *PyMultiNest: Python interface for MultiNest*, Astrophysics Source Code Library, record ascl:1606.005. <http://ascl.net/1606.005>
- Callister, T. A. 2024, arXiv e-prints, arXiv:2410.19145, doi: [10.48550/arXiv.2410.19145](https://doi.org/10.48550/arXiv.2410.19145)
- Callister, T. A., & Farr, W. M. 2024, *Physical Review X*, 14, 021005, doi: [10.1103/PhysRevX.14.021005](https://doi.org/10.1103/PhysRevX.14.021005)
- Callister, T. A., Haster, C.-J., Ng, K. K. Y., Vitale, S., & Farr, W. M. 2021, *ApJL*, 922, L5, doi: [10.3847/2041-8213/ac2ccc](https://doi.org/10.3847/2041-8213/ac2ccc)
- Cook, H. E., McKernan, B., Ford, K. E. S., et al. 2024, arXiv e-prints, arXiv:2411.10590, doi: [10.48550/arXiv.2411.10590](https://doi.org/10.48550/arXiv.2411.10590)
- Edelman, B., Doctor, Z., Godfrey, J., & Farr, B. 2022, *ApJ*, 924, 101, doi: [10.3847/1538-4357/ac3667](https://doi.org/10.3847/1538-4357/ac3667)
- Edelman, B., Farr, B., & Doctor, Z. 2023, *ApJ*, 946, 16, doi: [10.3847/1538-4357/acb5ed](https://doi.org/10.3847/1538-4357/acb5ed)
- Essick, R., & Farr, W. 2022, arXiv e-prints, arXiv:2204.00461, doi: [10.48550/arXiv.2204.00461](https://doi.org/10.48550/arXiv.2204.00461)
- Farmer, R., Renzo, M., de Mink, S. E., Marchant, P., & Justham, S. 2019, *ApJ*, 887, 53, doi: [10.3847/1538-4357/ab518b](https://doi.org/10.3847/1538-4357/ab518b)
- Farr, W. M. 2019, *Research Notes of the American Astronomical Society*, 3, 66, doi: [10.3847/2515-5172/ab1d5f](https://doi.org/10.3847/2515-5172/ab1d5f)
- Fishbach, M., Kimball, C., & Kalogera, V. 2022, *ApJL*, 935, L26, doi: [10.3847/2041-8213/ac86c4](https://doi.org/10.3847/2041-8213/ac86c4)
- Gerosa, D., & Fishbach, M. 2021, *Nature Astronomy*, 5, 749, doi: [10.1038/s41550-021-01398-w](https://doi.org/10.1038/s41550-021-01398-w)
- Godfrey, J., Edelman, B., & Farr, B. 2023, arXiv e-prints, arXiv:2304.01288, doi: [10.48550/arXiv.2304.01288](https://doi.org/10.48550/arXiv.2304.01288)
- Guo, W.-H., Li, Y.-J., Wang, Y.-Z., et al. 2024, *ApJ*, 975, 54, doi: [10.3847/1538-4357/ad758a](https://doi.org/10.3847/1538-4357/ad758a)
- Heinzel, J., Vitale, S., & Biscoveanu, S. 2024, *PhRvD*, 109, 103006, doi: [10.1103/PhysRevD.109.103006](https://doi.org/10.1103/PhysRevD.109.103006)
- Li, G.-P., & Fan, X.-L. 2024, arXiv e-prints, arXiv:2411.09195, doi: [10.48550/arXiv.2411.09195](https://doi.org/10.48550/arXiv.2411.09195)
- Li, Y.-J., Tang, S.-P., Gao, S.-J., Wu, D.-C., & Wang, Y.-Z. 2024a, *ApJ*, 977, 67, doi: [10.3847/1538-4357/ad83b5](https://doi.org/10.3847/1538-4357/ad83b5)
- Li, Y.-J., Wang, Y.-Z., Han, M.-Z., et al. 2021, *ApJ*, 917, 33, doi: [10.3847/1538-4357/ac0971](https://doi.org/10.3847/1538-4357/ac0971)
- Li, Y.-J., Wang, Y.-Z., Tang, S.-P., & Fan, Y.-Z. 2024b, *PhRvL*, 133, 051401, doi: [10.1103/PhysRevLett.133.051401](https://doi.org/10.1103/PhysRevLett.133.051401)
- Li, Y.-J., Wang, Y.-Z., Tang, S.-P., et al. 2022, *ApJL*, 933, L14, doi: [10.3847/2041-8213/ac78dd](https://doi.org/10.3847/2041-8213/ac78dd)
- Madau, P., & Dickinson, M. 2014, *ARA&A*, 52, 415, doi: [10.1146/annurev-astro-081811-125615](https://doi.org/10.1146/annurev-astro-081811-125615)
- Mandel, I., & Farmer, A. 2022, *PhR*, 955, 1, doi: [10.1016/j.physrep.2022.01.003](https://doi.org/10.1016/j.physrep.2022.01.003)
- Mandel, I., Farr, W. M., & Gair, J. R. 2019, *MNRAS*, 486, 1086, doi: [10.1093/mnras/stz896](https://doi.org/10.1093/mnras/stz896)
- McKernan, B., Ford, K. E. S., Callister, T., et al. 2022, *MNRAS*, 514, 3886, doi: [10.1093/mnras/stac1570](https://doi.org/10.1093/mnras/stac1570)
- McKernan, B., Ford, K. E. S., Bellovary, J., et al. 2018, *ApJ*, 866, 66, doi: [10.3847/1538-4357/aadae5](https://doi.org/10.3847/1538-4357/aadae5)
- Olejak, A., Klencki, J., Xu, X.-T., et al. 2024, *A&A*, 689, A305, doi: [10.1051/0004-6361/202450480](https://doi.org/10.1051/0004-6361/202450480)
- Payne, E., Kremer, K., & Zevin, M. 2024, *ApJL*, 966, L16, doi: [10.3847/2041-8213/ad3e82](https://doi.org/10.3847/2041-8213/ad3e82)
- Ray, A., Magaña Hernandez, I., Breivik, K., & Creighton, J. 2024, arXiv e-prints, arXiv:2404.03166, doi: [10.48550/arXiv.2404.03166](https://doi.org/10.48550/arXiv.2404.03166)

- Santini, A., Gerosa, D., Cotesta, R., & Berti, E. 2023, PhRvD, 108, 083033, doi: [10.1103/PhysRevD.108.083033](https://doi.org/10.1103/PhysRevD.108.083033)
- Talbot, C., & Golomb, J. 2023, MNRAS, 526, 3495, doi: [10.1093/mnras/stad2968](https://doi.org/10.1093/mnras/stad2968)
- Talbot, C., & Thrane, E. 2018, ApJ, 856, 173, doi: [10.3847/1538-4357/aab34c](https://doi.org/10.3847/1538-4357/aab34c)
- Tiwari, V. 2022, ApJ, 928, 155, doi: [10.3847/1538-4357/ac589a](https://doi.org/10.3847/1538-4357/ac589a)
- Tiwari, V., & Fairhurst, S. 2021, ApJL, 913, L19, doi: [10.3847/2041-8213/abf7e7](https://doi.org/10.3847/2041-8213/abf7e7)
- Wang, Y.-Z., Li, Y.-J., Vink, J. S., et al. 2022, ApJL, 941, L39, doi: [10.3847/2041-8213/aca89f](https://doi.org/10.3847/2041-8213/aca89f)
- Yang, Y., Bartos, I., Gayathri, V., et al. 2019, PhRvL, 123, 181101, doi: [10.1103/PhysRevLett.123.181101](https://doi.org/10.1103/PhysRevLett.123.181101)
- Zevin, M., & Holz, D. E. 2022, ApJL, 935, L20, doi: [10.3847/2041-8213/ac853d](https://doi.org/10.3847/2041-8213/ac853d)
- Zevin, M., Bavera, S. S., Berry, C. P. L., et al. 2021, ApJ, 910, 152, doi: [10.3847/1538-4357/abe40e](https://doi.org/10.3847/1538-4357/abe40e)